JOURNAL OF MATERIALS SCIENCE 17 (1982) 861–865

Electron microscopy study of crystallization behaviour of $Fe_{40}Ni_{38}Mo_4B_{18}$ (2826 MB) metallic glass

F. L. CUMBRERA, M. MILLÁN, A. CONDE, R. MÁRQUEZ
Departamento de Optica y Sección de Física del Centro Coordinado del CSIC, Universidad de Sevilla, Spain

P. VIGIER
Groupe de Metallurgie Physique, ERA 238, Faculté des Sciences de Rouen, France

Crystallization behaviour of 2826 MB metglas has been studied by transmission electron microscopy and selected area diffraction. Dynamic heating between room temperature and 1100 K and isothermal annealing close to crystallization onset have been performed. Crystallization takes place through a two-stage process to give MSI and MSII phases and details of these are discussed. A new transformation to a stable phase SIII is detected in agreement with the third peak observed by differential thermal analysis experiments.

1. Introduction

The glass alloy of nominal composition $Fe_{40}Ni_{38}Mo_4B_{18}$ (Metglas 2826 MB), which contains boron as the only metalloid, was developed after the observation that the complex Fe–Ni–P–B glassy alloy exhibited magnetic and thermal instabilities which seem to be a common characteristic of the non-crystalline magnetic alloys containing phosphorous as the major metalloid [1, 2]. The thermal stability is an improvement of its remarkable soft-magnetic properties. Azam *et al.* [3] have reported an earlier study on the crystallization of this Metglas and have studied some irradiation effects. However, detailed studies of the physical properties and crystallization of this alloy are lacking. In a previous paper [4] the authors have studied, through magnetic susceptibility, calorimetry and electrical resistivity measurements, some parameters related to crystallization and crystallization kinetics, but a structural study of the crystallization was needed. The present work is thus concerned mainly with characterization of crystallization morphologies and the equilibrium and intermediary crystalline phases by electron microscopy and diffraction.

2. Experimental procedure

For transmission electron microscopy (TEM), pieces of about 0.5 cm long were cut from Metglas ribbons and then electrolytically thinned in an electrolyte consisting of 80 vol% acetic acid and 20 vol% perchloric acid. The temperature of the electrolyte was maintained at 290 K and the applied voltage was 30 V. The TEM examination was performed in Philips EM-300 and JEM-100C electron microscopes, both equipped with a heating holder and a tilt-rotation holder.

Room temperature experiments were performed and also the thermal evolution of the structure was investigated. Two types of experiments were carried out: dynamic heating at several rates and isothermal annealing at different temperatures below the crystallization temperature.

3. Results

3.1. Amorphous samples

At room temperature, electron micrographs of 2826 MB alloys (Fig. 1) show structureless features except for a fine pseudo-grain structure which disappears at some stage of thermal treatment. This kind of pseudo-grain structure has been

0022–2461/82/030861–06$03.22/0

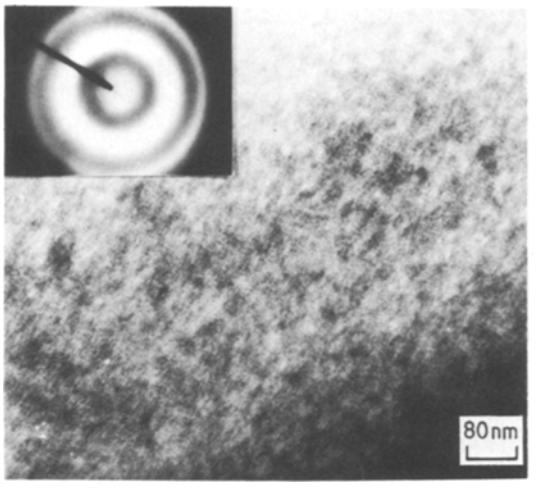

Figure 1 TEM micrograph and SAD pattern of 2826 MB alloy at room temperature, indicating amorphous structure.

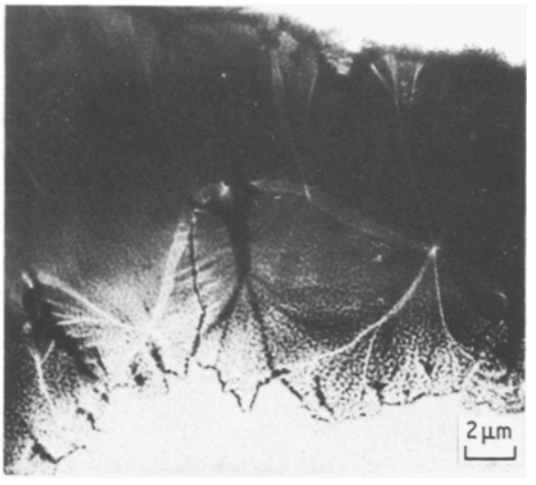

Figure 3 Lorentz micrograph of unannealed foil of 2826 MB alloy.

observed in other amorphous alloys containing Ni and considered as an artifact due to electropolishing [5]. There is no evidence of dislocations, grain boundaries, stacking faults or other features of crystalline metallic specimens. Dark-field techniques also showed no grain structure. The diffraction pattern, showing broad diffuse liquid-like haloes, provide evidence for amorphous structure. The first halo is the strongest and the second halo shows the characteristic shoulder in its high-angle side. Both are typical features of diffraction patterns of metallic glasses. As pointed out by Azam *et al.* [3] the position of amorphous haloes is related to the crystalline rings which appear in the early stage of crystallization. However, higher magnification micrographs of very thin sections exhibited very small grains of crystalline appearance with sizes between 3.0 and 7.5 nm or even less, as shown in Fig. 2.

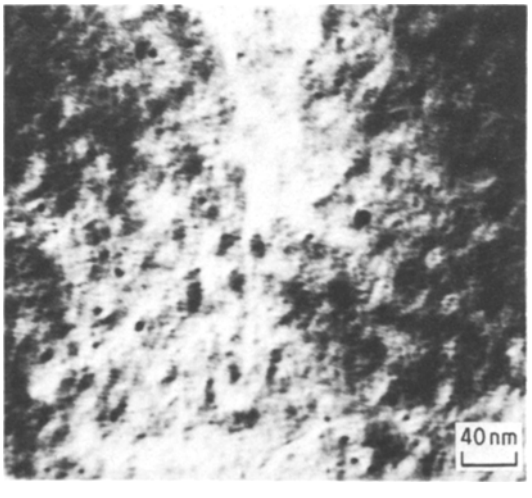

Figure 2 Electron micrograph at room temperature and higher magnification showing small grains.

Fig. 3 is a typical Lorentz micrograph of this ferromagnetic material containing Bloch walls, Bloch lines, flux closure domains, and typical circularly magnetized domain patterns which have been observed in magnetic high permeability alloys [6]. The domain walls are sometimes not definitely observed, and, especially at outer parts of the specimen, they vanish. This can be due to the thickness of the sample but it seems also a consequence of the small anisotropy of these materials. In fact, the lower the anisotropy is, the wider the domain wall becomes and, in the limit of zero anisotropy, domain walls cannot be defined. This may correspond to the above case. These star-like domain patterns observed have been previously reported [7] for 2605 ($Fe_{80}B_{20}$) alloy and were attributed to dilatational stress centres generated during the quenching process. By tilting the holder it is possible to observe domain wall motion associated with different magnetization processes. The drastic change of magnetization which gives the hysteresis loop its characteristic rectangular shape is manifested by a sudden change of the domain wall pattern when the magnetization is inverted.

When a sample is heated, prior to the nucleation of crystalities, a coarsening of fine structure is usually observed in bright-field TEM images.

This observed coarsening is most likely related to atomic arrangements occurring below the crystallization temperature, generally known as "structural relaxation process". Structural and compositional rearrangement is possible at temperatures just below T_g because it is expected that atomic transport properties would decrease at relatively slow rates as T decreases below T_g [8]. Also it is shown that diffusivity for some elements has an activation energy three or four times smaller than the apparent activation energy for viscous flow in the T_g range [9]. Diffraction patterns show apparently no evidence of change but it was shown previously [10, 11] by quantitative analysis that these patterns lead to some differences in the interference function.

As expected from the above assumptions, crystallization nature is markedly influenced by previous thermal history of the material such as thermal treatments and different heating rates, and so the crystallization results are separated in two different paragraphs: crystallization under dynamic heating and crystallization under isothermal annealings.

3.2. Crystallization under dynamic heating

The first sign of the crystallization onset is a noticeable intensification on the low-angle side of the first amorphous halo to give the (1 1 1) ring of a fcc structure (MSI), and then (200), (220), (3 1 1), etc., reflections appear. Fig. 4 shows a micrograph of the early crystallization stage (nucleation and growth of MSI nuclei is in progress) and the corresponding selected area diffraction (SAD) pattern. Crystallographic analysis shows that MSI crystals correspond to the iron–nickel fcc solid solution (austenite-type), with a lattice parameter $a \sim 0.354$ nm. It is noteworthy that room-temperature diffraction patterns of crystallites that sometimes exist embedded in the amorphous structure area of the MSI type but with a larger lattice parameter (even $a \sim 0.365$ nm) showing a more relaxed structure compatible with free volume in amorphous structure.

Near the second crystallization temperature there is a remarkable sudden appearance of copious spherulite-like domains with some ordering in their repartition. SAD patterns, however, show no evidence of phase transformation and tilting experiments do not show contrast change in these domains (Fig. 5). A short time later, a sharpening of these domains is accompanied by the appearance of a new phase (MSII) in the diffraction patterns as shown by Fig. 6.

MSI crystals nucleate copiously but grow slowly. MSII crystals are larger than those of the MSI type and their growth rate is also faster. They are fcc ($a = 1.047$ nm) and belong to a structure of the $Cr_{23}C_6$ type which we have identified as the $Fe_xNi_{23-x}B_6$ solid solution previously reported by Ayel *et al.* [12] who have extensively studied all the (FeNiB) solid solutions in the range 0 to 33.3 wt % B.

For higher temperatures a new transformation is observed manifested by long-range diffusion phenomena and an increase in thickness. The corresponding SAD patterns are complex and show Kikuchi lines and the stable phase SIII is

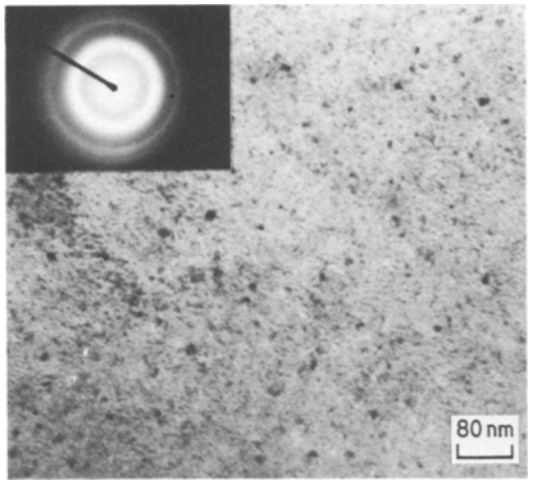

Figure 4 Electron micrograph and diffraction pattern of an area showing the early stage of crystallization.

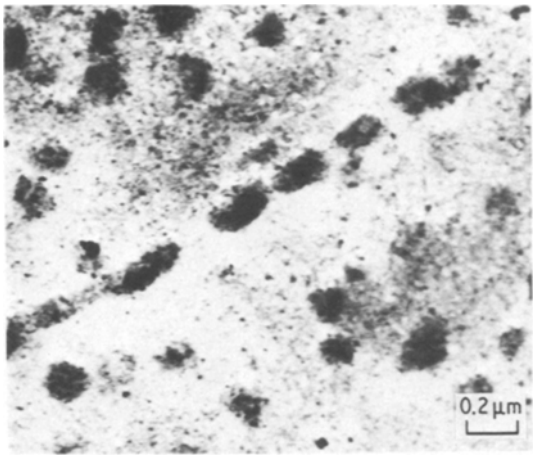

Figure 5 Distribution of spherulite-like domains near the second crystallization. Their repartition suggests some ordering of arrangement.

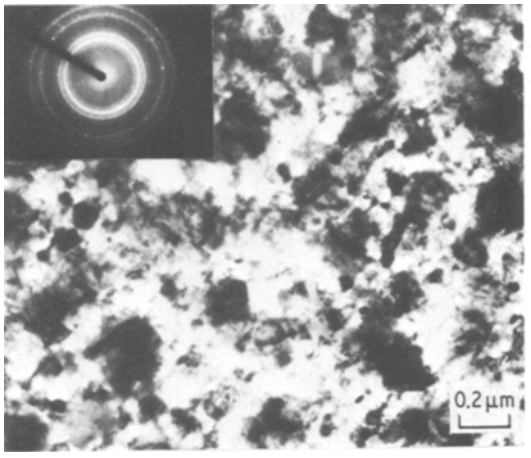

Figure 6 Bright-field image showing MSI and MSII crystals and associated SAD pattern.

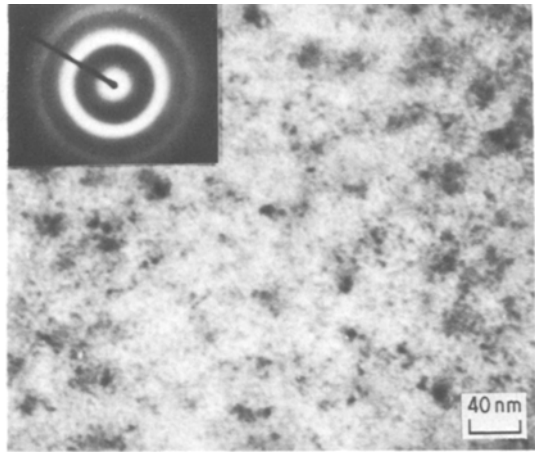

Figure 8 TEM micrograph and SAD pattern after 8 h of a "low temperature" isothermal annealing.

probably found. For very high heating rates experiments MSI and MSII crystals co-exist at 825 K, but the grain size is now very large (Fig. 7).

3.3. Crystallization under isothermal annealing

For samples heated under isothermal condition, transformations are more gradual than in dynamic experiments. Some differences between low-temperature annealing and annealing performed near the onset of the first crystallization are observed. For samples annealed at 575 K the presence of crystallites is detected after 50 min, although the sample is still predominantly amorphous. This result disagrees with the results of Azam *et al.* [3] who do not detect the presence of crystallites within two hours for the same temperature. After four hours the diffraction pattern clearly exhibits the fcc MSI typical diagram, but the amorphous phase still remains. Even after 8 h MSII crystals had not been observed (Fig. 8) and the amorphous phase still had not disappeared, but it did exhibit a transformed aspect. Fig. 9 shows a dark-field picture formed from the first ring of a sample heated for 2 h at 600 K. Crystals observed are of the MSI type and the amorphous phase remains.

For higher temperatures (650 K) nucleation starts with the MSI crystals but for longer annealing times the remaining amorphous matrix is transformed into some large MSII crystals. For annealing temperatures near the crystallization temperature (~ 700 K) MSII crystals are formed, even in the first instants, with the smaller MSI crystals. They

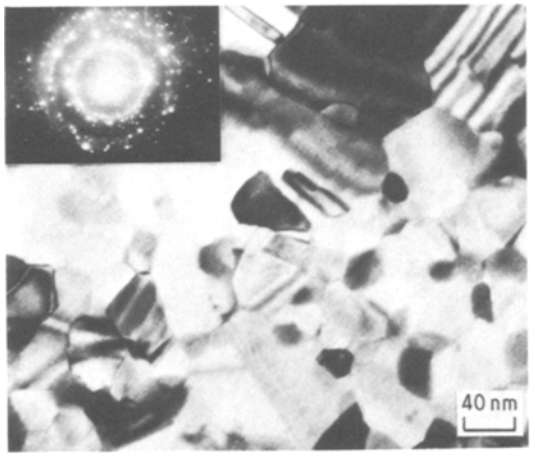

Figure 7 Grain structure after a high heating rate experiment and SAD pattern.

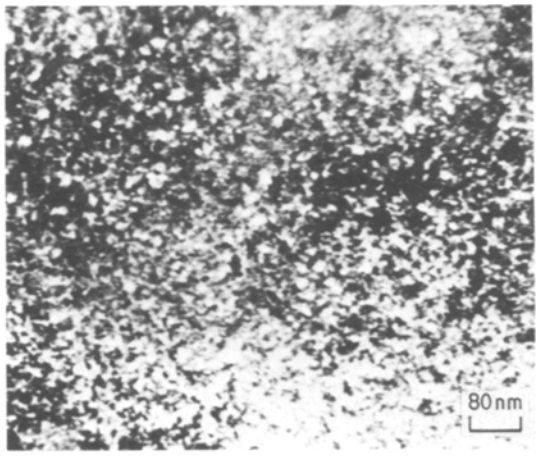

Figure 9 Dark-field image of a sample annealed for 2 h at 600 K, formed from a portion of the inside ring.

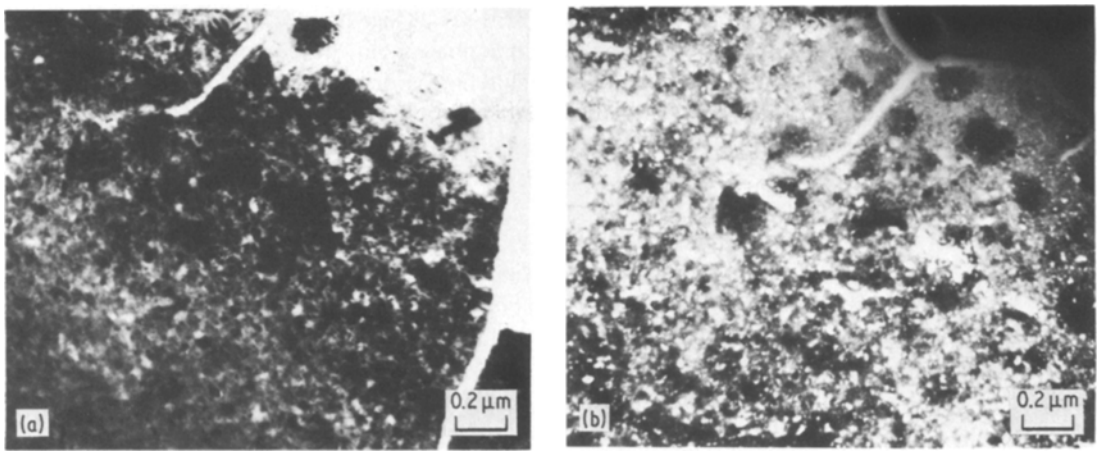

Figure 10 (a) Bright-field image showing annealing twins in MSII crystals and (b) the corresponding dark-field picture formed from the inside ring of MSII phase.

grow rapidly and many micro-twins are detected, as can be seen in the bright- and dark-field micrographs shown in Fig. 10. These micro-twins then coalesce into macro-twins or grow into a twin-free grain.

Fig. 11 shows a typical Lorentz micrograph of a sample after crystallization. A characteristic feature is the presence of ripples, absent in the amorphous images.

4. Discussion

Crystallization phenomena in this complex system exhibit some similarities to the crystallization of the complex system 2826 A ($Fe_{32}Ni_{36}Cr_{14}P_{12}B_6$) [13, 14]. The first formed MSI crystals are probably the result of a "primary" crystallization. As is known [13, 15], a crystal that forms initially in the glassy matrix is termed "polymorphous" if its composition is still the same as in the glassy state, and "primary" if the composition has changed drastically depending on the position of the alloy in the free enthalpy against concentration diagram.

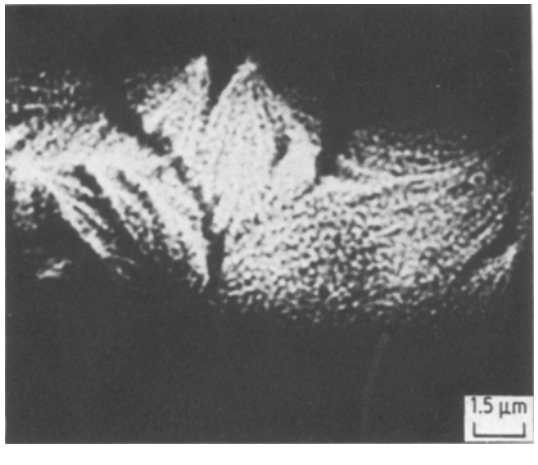

Figure 11 Lorentz image showing a detail of domain structure after crystallization.

In this case when "primary" crystallization occurs, a metastable equilibrium is established between a solid solution crystal phase having a higher metal concentration and the remaining glassy phase, which is enriched in the metalloid. Heimendahl *et al.* [13] have verified this assumption by X-ray microanalysis in the MSI crystallization of 2826 A alloy. In the present case "primary" crystallization should be the origin of the small changes in the lattice parameter of the MSI phase. It is supposed that during the MSI crystallization the metalloid B is removed and then the matrix is enriched in B. This fact could explain the appearance of spherulitic domains as B-rich regions in the glassy matrix. Thus the obvious necessity of the different subsequent MSII stage. MSII crystals grow quickly and their growth seems to occur by grain boundary migration or by twin plate formation. These twins later coalesce into twins of coarser size or they are annealed out. Thus, grain growth of MSII crystals does not occur by coalescence of neighbouring grains, as two drops of water coalesce.

Some peculiarities of this type of growth were observed: (a) a curved grain boundary usually migrates toward its centre of curvature and (b) where grain boundaries meet at angles other than 120° the grain included by the more acute angle will be consumed, so that all angles approach 120°.

The recrystallization twins are among the most prominent features of recrystallized face-centred cubic metals [16]. These usually appear as parallel-sided bands that run across the grains, the parallel boundaries coinciding with (1 1 1) twinning planes. Generally coherent boundaries are observed but sometimes non-coherent boundaries also appear where a twin terminates within a grain. Interfaces between MSI crystals and the amorphous matrix should be stressed or deformed parts, where numerous stacking faults would be formed when MSII crystals develop. This growth accident generates twins later. When a grain gets a new neighbour, the formation of a twin on any possible plane in the growing plane will be allowed, whenever that twinned orientation presents advantages, i.e., permitting a grain boundary configuration having lower interfacial energy.

Generally, the phenomenon can be interpreted as analogous to the formation of non-equilibrium carbides in Cr–C binary alloys, having 13 to 22 wt% carbon, when quenched rapidly from the melt. In this case bcc chromium and the non-equilibrium Cr_3C (orthorhombic, Fe_3C type) are obtained, but upon tempering Cr_3C transforms into the equilibrium phase $Cr_{23}C_6$ via a metastable Cr_7C_3 phase. As it is known, MSII crystals are isomorphous with the $Cr_{23}C_6$ phase, which gives large crystals and has a complex structure with a large unit cell volume. Thus, the long-range atomic rearrangements required for the nucleation of $Cr_{23}C_6$ crystals will be more difficult in the early stage of crystallization, and this phase is not developed until after recrystallization.

Finally, for higher temperatures a new transformation occurs. The spot diffraction pattern is not simple but it corresponds to the MSII (fcc) phase, with a slightly modified lattice parameter, together with some unidentified faint spots. When the sample is heated at higher temperatures it is supposed that the MSI small crystals are consumed by the larger MSII ones and an MSII (fcc) structure with a slightly larger lattice parameter is arrived at. In the new phase there is a lower metalloid content than MSII phase and, if it is assumed that metalloid atoms occupy interstitial positions of a compact fcc structure, now a more relaxed stable structure is obtained. This last transformation should correspond to the third peak observed in DTA experiences [18].

Long-range diffusion is needed for this transformation and because the samples studied by TEM are wedge-shaped a matter flux is observed sometimes from the border to the inner regions. This fact is due to the lower proportion of MSII large crystals in the thin borders of the samples and because of this diffusion effect, thickness is increased, as observed in TEM micrographs.

Crystallization under dynamic heating has, as seen, a parallel behaviour to the annealing of cold-worked metals. However, the more gradual crystallization under isothermal annealing is more similar to the precipitaction of supersaturated solid solutions where the more stable phases are usually the last to form [5].

References

1. R. HASEGAWA, M. C. NARASIMHAN and N. DE CRISTOFARO, *J. Appl. Phys.* **49** (1978) 1712.
2. F. LUBORSKY, Proceedings of the 21st Annual Conference on Magnetism and Magnetic Materials, AIP Conference Proceedings number 29 (American Institute of Physics, 1976) p. 209.
3. N. AZAM, L. LE NAOUR, C. RIVERA, P. GROSJEAN, P. SACOVY and J. DELAPLACE, *J. Nucl. Mater.* **83** (1979) 298.
4. F. L. CUMBRERA, H. MIRANDA, P. VIGIER, A. CONDE and R. MARQUEZ, to be published.
5. H. CHANG and S. SASTRI, *Met. Trans.* **A8** (1977) 1063.
6. Y. NAKAGAWA, *J. Phys. Soc. Japan* **30** (1971) 1596.
7. G. SCHROEDER, R. SCHÄFER and H. KRONMÜLLER, *Phys. Stat. Sol. a* **50** (1978) 475.
8. R. RAY, Ph. D. Thesis. MIT, Cambridge, Mass (1969).
9. J. M. VITEK, Ph. D. Thesis. MIT, Cambridge, Mass (1973).
10. F. L. CUMBRERA, P. VIGIER and J. MALANDAIN, *C. R. Acad. Sci. Paris* **288** (1979) 383.
11. F. L. CUMBRERA and P. VIGIER, *Phys. Stat. Sol. a* **63** (1981) 631.
12. M. AYEL, R. RIVIERE and G. MONNIER, *C. R. Acad. Sci. Paris* **C264** (1967) 1756.
13. M. HEIMENDAHL and H. OPPOLZER, *Scripta Metal.* **12** (1978) 1087.
14. M. HEIMENDAHL and G. MAUSSNER, *J. Mater. Sci.* **14** (1979) 1238.
15. U. KOSTER, *Act. Metal.* **20** (1972) 1361.
16. J. E. BURKE and D. TURNBULL, in "Progress in Metals Physics" Vol. 3, edited by B. Chalmers (Pergamon Press, London, 1952) p. 220.
17. A. INOUE and T. MASUMOTO, *Scripta Metal.* **13** (1979) 711.
18. A. K. MAJUMDAR and A. K. NIGAM, *J. Appl. Phys.* **51** (1980) 4218.

Received 17 June
and accepted 16 August 1981